GEOPHYSICS, VOL. 87, NO. 3 (MAY-JUNE 2022); P. MR117–MR128, 17 FIGS., 1 TABLE.
10.1190/GEO2021-0542.1

DOI:10.1190/geo2021-0542.1

Reflection and transmission of thermoelastic waves in multilayered media

Wanting Hou[1], Li-Yun Fu[2], and Jose M. Carcione[3]

ABSTRACT

In many cases, multilayered media with flat interfaces are a suitable representation of the geologic features of the crust. In general, the isothermal theory is used, and the transfer-matrix (TM) method is applied to compute the scattering reflection and transmission (R/T) coefficients. We have generalized the TM algorithm to the more general case of thermoelastic layers, in which elastic waves give rise to a temperature field (the thermal [T] wave) and vice versa. The stress-strain relation is based on the Lord-Shulman (LS) thermoelasticity theory. Then, the R/T coefficients of the fast compressional (P), T, and shear (S) waves are computed and verified by the conservation of energy. We also obtain the energy ratios and phase angles for P- and S-wave incidences. We consider a hot dry rock (HDR) geothermal model to study the effects of temperature, frequency, and layer thickness, and we find that the coefficients potentially can be used to obtain information about the characteristics of a multilayered medium.

INTRODUCTION

The theory of thermoelasticity combines the equation of dynamic elasticity with that of heat conduction, whereby deformation-temperature coupling terms are taken into account. Including the temperature field is of interest in many applications, such as seismology and geothermal exploration (Boschi, 1973; Jacquey et al., 2015). A promising practical application of thermoelasticity studies geothermal energy produced from hot dry rocks (HDRs) (e.g., Brown et al., 2012).

Biot (1956) develops a classic theory based on the thermodynamics of irreversible processes, which predicts a slow thermal P mode (or T-wave) besides the fast compressional (P) and shear (S) waves. The characteristics of the T-wave are analogous to the slow P-wave in poroelasticity, which is the low-frequency diffusive and high-frequency wave-like behaviors. Moreover, the existence of it has been confirmed experimentally in solid helium (Ackerman et al., 1966) and sodium fluoride crystals (McNelly et al., 1970). Biot's theory has been improved by Lord and Shulman (1967) (LS theory) and Green and Lindsay (1972) (GL theory), who modify the Fourier heat-conduction equation by introducing relaxation times (Eslami et al., 2013). (The latter introduces additional relaxation times compared to the LS theory.) These models predict thermoelastic wave propagation with finite velocities avoiding the infinite values of the classic theory. Green's functions from these new equations have been obtained (Nowacki, 1975; Wang et al., 2020b), and numerical methods have been developed to compute thermoelasticity fields (Tehrani and Mohamad, 2000) and the first simulation of the T-wave in heterogeneous media (Carcione et al., 2019a, 2019b; Hou et al., 2021a). These numerical algorithms require proper verification, with the first choice being the comparison of the fields with the Green's functions (homogeneous media) and subsequently with more general semianalytical solutions, such as those corresponding to multilayered media.

Thomson (1950) and Haskell (1953) introduce the transfer-matrix (TM) algorithm for reflection and transmission (R/T) of elastic waves in layered isotropic isothermal media. The method has been used by Bufler (1971) and Bahar (1972), and Bahar and Hetnarski (1980) consider thermoelasticity problems. Potel and Belleval (1993) and Vashishth and Khurana (2004) provide further insight into the anisotropic case. Ai et al. (2015) use a different technique, that is, an eigenvalue approach to study the effects of the layers on thermoelasticity. However, these studies are based on the classical (parabolic) Fourier heat conduction law, whereas the generalized theories contain a relaxation term leading to a more physical (hyperbolic) heat equation and finite velocities, as mentioned previously. Many works consider thermoelasticity with relaxation terms to study wave propagation at interfaces. Sinha and Elsibai (1996) use the GL theory, whereas

Manuscript received by the Editor 18 August 2021; revised manuscript received 28 November 2021; published ahead of production 31 January 2022; published online 8 March 2022.
[1]China University of Petroleum (East China), Key Laboratory of Deep Oil and Gas, Qingdao 266580, China. E-mail: hwtupc@163.com.
[2]China University of Petroleum (East China), Key Laboratory of Deep Oil and Gas, Qingdao 266580, China and Qingdao National Laboratory for Marine Science and Technology, Laboratory for Marine Mineral Resources, Qingdao 266071, China. E-mail: lfu@upc.edu.cn (corresponding author).
[3]National Institute of Oceanography and Applied Geophysics (INOGS), Trieste 34010, Italy and Hohai University, Nanjing 210098, China. E-mail: jose.carcione@gmail.com.

Chakraborty and Singh (2011) investigate the effects of initial stress. Recently, Kaur et al. (2020) consider the reflection and refraction problem at a piezo-thermoelastic interface, and Wang et al. (2020a, 2021) consider an incident inhomogeneous plane wave on a thermally insulated free surface of a porous medium and the surface of a thermo-poroelastic medium, respectively, where the results are verified with an energy balance.

We compute the scattering R/T coefficients in multilayered thermoelastic media based on the LS theory by applying the TM method. Two longitudinal waves (P and T) and one S-wave are reflected and transmitted. Unlike the elastic case, dissipation implies the presence of inhomogeneous waves, that is, the directions of the wavenumber and attenuation vectors do not coincide. We use potential functions to describe the waves and suitable boundary conditions. The validity of the coefficients is verified by an energy balance (conservation of energy). Moreover, we consider an HDR system and study how temperature, frequency, and layered thickness affect the coefficients.

FUNDAMENTAL EQUATIONS

Biot (1956) introduces the constitutive relations of thermoelasticity as

$$\sigma_{ij} = 2\mu\epsilon_{ij} + \delta_{ij}(\lambda\epsilon - \bar{\gamma}T), \tag{1}$$

where σ_{ij} and ϵ_{ij} ($\epsilon = \epsilon_{ii}$; $i, j = x, y, z$, Einstein summation assumed) are the components of the stress and strain tensors, respectively; T is the increment of temperature above a reference absolute temperature T_0 at zero stress and strain state; λ and μ are the Lamé constants of the medium; δ_{ij} are the Kronecker-delta functions; and $\bar{\gamma} = (3\lambda + 2\mu)\bar{\alpha}$ is the thermal modulus, where $\bar{\alpha}$ is the linear thermal expansion coefficient. If $\bar{\alpha} = 0$, the P- and T-waves are uncoupled. The strain-displacement relations are

$$2\epsilon_{ij} = u_{i,j} + u_{j,i}, \tag{2}$$

where u_i (or u_j) denote the components of the displacement field in the i (or j) direction, and the subscript "$,i$" (or "$,j$") denotes the spatial derivative with respect to x_i (or x_j). However, the equations of momentum conservation are

$$\sigma_{ij,j} = \rho\ddot{u}_i, \tag{3}$$

where ρ is the material density and the dot above a variable denotes time differentiation.

Substituting equation 1 into equation 3 and using the strain-displacement relations equation 2, we obtain the displacement equations of motion and law of heat conduction, based on the LS theory (Lord and Shulman, 1967; Carcione et al., 2019a):

$$\begin{aligned}&(\lambda+\mu)\nabla(\nabla\cdot\mathbf{u}) + \mu\nabla^2\mathbf{u} - \bar{\gamma}\nabla T - \rho\ddot{\mathbf{u}} = 0,\\ &\bar{\kappa}\nabla^2 T = c(\dot{T} + \tau\ddot{T}) + \bar{\gamma}T_0\nabla\cdot(\dot{\mathbf{u}} + \tau\ddot{\mathbf{u}}),\end{aligned} \tag{4}$$

respectively, where $\mathbf{u} = (u_x, u_y, u_z)$, c is the specific heat of the unit volume in the absence of deformation, $\bar{\kappa}$ is the coefficient of thermal conduction, and the heat source is not included. The law of heat conduction in the LS theory is hyperbolic due to the presence of the relaxation time τ (e.g., Rudgers, 1990).

Using the Helmholtz decomposition, we have

$$\mathbf{u} = \nabla\phi + \nabla\times(\psi\hat{\mathbf{n}}), \nabla\cdot(\psi\hat{\mathbf{n}}) = 0, \tag{5}$$

where ϕ and $\psi\hat{\mathbf{n}}$ are the potentials, with a hat denoting a unit vector. Substituting the two potentials into equation 4 yields

$$\bar{\gamma}T = (\lambda + 2\mu)\nabla^2\phi - \rho\ddot{\phi}, \tag{6a}$$

$$\bar{\kappa}\nabla^2 T - c(\dot{T} + \tau\ddot{T}) = \bar{\gamma}T_0\nabla^2(\dot{\phi} + \tau\ddot{\phi}), \tag{6b}$$

$$\mu\nabla^2\psi - \rho\ddot{\psi} = 0. \tag{6c}$$

We consider the following plane-wave solutions of the Helmholtz equation:

$$[\phi, T, \psi] = [A_\phi, A_T, A_\psi]\exp[\mathrm{i}(\omega t - \mathbf{k}\cdot\mathbf{x})], \tag{7}$$

which defines the propagation of P, T, and S attenuated thermoelastic plane waves with amplitudes A_ϕ, A_T, and A_ψ, complex wavenumber vector $\mathbf{k}$ (or wavevector), and angular frequency ω ($\mathrm{i}^2 = -1$), where

$$\begin{aligned}\mathbf{k} &= \kappa\hat{\boldsymbol{\kappa}} - \mathrm{i}\alpha\hat{\boldsymbol{\alpha}},\\ \hat{\boldsymbol{\kappa}} &= (\sin\theta, \cos\theta),\\ \hat{\boldsymbol{\alpha}} &= (\sin(\theta-\gamma), \cos(\theta-\gamma)),\end{aligned} \tag{8}$$

where θ is the propagation angle and γ is the inhomogeneity angle between $\hat{\boldsymbol{\kappa}}$ and $\hat{\boldsymbol{\alpha}}$. If we assume incident homogeneous plane waves ($\gamma = 0°$), the wavenumber and complex velocity are

$$\begin{aligned}\mathbf{k} &= (\kappa - \mathrm{i}\alpha)\hat{\boldsymbol{\kappa}} = k\hat{\boldsymbol{\kappa}},\\ V_c &= \frac{\omega}{k},\end{aligned} \tag{9}$$

respectively.

Substituting equations 7 and 8 into 6c, we obtain the S-wave velocity

$$V_S = \sqrt{\frac{\mu}{\rho}}, \tag{10}$$

where we can see that thermal effects have no influence on the S-wave in homogeneous media.

Similarly, the solution for the two P-waves, using equations 6a, 6b, and 7, can be obtained from the following dispersion equation:

$$\mathbf{L}\cdot\mathbf{KP} = 0, \tag{11}$$

where

$$\begin{aligned}&\mathbf{L} = [\,L_0 \quad (L_1+L_2)\omega^2 \quad \omega^4\,], \quad \mathbf{KP} = [\,k^4 \quad k^2 \quad 1\,]^{\mathrm{T}},\\ &k^2 = \frac{\omega^2}{2L_0}\left[-(L_1+L_2) \pm \sqrt{(L_1+L_2)^2 - 4L_0}\right],\end{aligned} \tag{12}$$

for which the minus and plus are applicable when taking the square root k^2 corresponds to the fast P- and T-waves, respectively, and

$$L_0 = -V_0^2 L_2,$$
$$L_1 = -\left(V_0^2 + \frac{\bar{\gamma}^2}{\rho c} T_0\right),$$
$$L_2 = \frac{\omega\bar{\kappa}}{c(\mathrm{i} - \tau\omega)},$$
$$V_0^2 = \frac{\lambda + 2\mu}{\rho}. \tag{13}$$

The P- and T-wave wavenumbers are obtained from

$$k^2 = \mathbf{k}\cdot\mathbf{k},$$
$$\mathrm{Re}(k^2) = \kappa^2 - \alpha^2,$$
$$\mathrm{Im}(k^2) = -2\kappa\alpha\cos\gamma. \tag{14}$$

We have (Carcione, 2014, equation 3.34):

$$\kappa^2 = \frac{1}{2}\left[\mathrm{Re}(k^2) + \sqrt{[\mathrm{Re}(k^2)]^2 + [\mathrm{Im}(k^2)]^2\sec^2\gamma}\right],$$
$$\alpha^2 = \frac{1}{2}\left[-\mathrm{Re}(k^2) + \sqrt{[\mathrm{Re}(k^2)]^2 + [\mathrm{Im}(k^2)]^2\sec^2\gamma}\right]. \tag{15}$$

The phase velocities of the P-waves, using equations 9 and 15, are

$$V_{\mathrm{ph}}^{\mathrm{ho}} = \left[\mathrm{Re}\left(\frac{1}{V_c}\right)\right]^{-1}, \quad V_{\mathrm{ph}}^{\mathrm{in}} = \frac{\omega}{\kappa}, \tag{16}$$

where the homogeneous and inhomogeneous waves are identified by the superscripts "ho" and "in," respectively. The attenuation coefficients of the P- and T-waves are given by

$$A^{\mathrm{ho}} = -\omega\mathrm{Im}\left(\frac{1}{V_c}\right), \quad A^{\mathrm{in}} = \alpha. \tag{17}$$

An alternative attenuation coefficient is that of Deresiewicz (1957):

$$L = 4\pi\frac{AV_{\mathrm{ph}}}{\omega}. \tag{18}$$

R/T COEFFICIENTS

Let us consider a 2D multilayered medium in the (x, z) plane, which consists of n media, including $n-2$ flat layers and two homogeneous half-spaces, as depicted in Figure 1a. The incidence medium is one ($z > 0$). Each layer has six waves, three upward and three downward; the upper half-space has four waves, three upward (the reflected ones) and one downward (the incident one), whereas the lower half-space has three propagating downward (transmitted) waves.

We assume the following: (1) each layer is isotropic and homogeneous and (2) the boundary conditions at the interfaces are the continuity of normal ($u_z = u_z'$) and tangential displacements ($u_x = u_x'$), normal ($\sigma_{zz} = \sigma_{zz}'$) and tangential stresses ($\sigma_{xz} = \sigma_{xz}'$), and temperature ($T = T'$) and heat flux ($\bar{\kappa}(\partial T/\partial z) = \bar{\kappa}\prime(\partial T'/\partial z)$) (e.g., Ignaczak and Ostoja-Starzewski, 2009).

At the ith layer, we assume that the velocities, density, and thickness are $V_{\mathrm{E}}^{(i)}$, $V_{\mathrm{T}}^{(i)}$, $V_{\mathrm{S}}^{(i)}$, $\rho^{(i)}$, and $h^{(i)}$, respectively, and the angles between the P-, S-, and T-wave vectors and the normal direction are $\theta_1^{(i)}$, $\theta_2^{(i)}$, and $\theta_3^{(i)}$, as shown in Figure 1b. The potential functions, based on the Snell law, are

$$\phi^{(i)} = \left[A_1^{(i)}e^{\mathrm{i}d^{(i)}z} + A_2^{(i)}e^{-\mathrm{i}d^{(i)}z} + C_1^{(i)}e^{\mathrm{i}l^{(i)}z} + C_2^{(i)}e^{-\mathrm{i}l^{(i)}z}\right]e^{\mathrm{i}(\omega t - \xi x)},$$
$$\psi^{(i)} = \left[B_1^{(i)}e^{\mathrm{i}s^{(i)}z} + B_2^{(i)}e^{-\mathrm{i}s^{(i)}z}\right]e^{\mathrm{i}(\omega t - \xi x)}, \tag{19}$$

where $A_m^{(i)}$, $B_m^{(i)}$, and $C_m^{(i)}$ are the amplitudes of the P-, S-, and T-waves, respectively; the superscript (i) denotes the properties of the ith layer; $m = 1$ represents the downward waves; $m = 2$ represents the upward waves; ξ is the horizontal wavenumber; and $d^{(i)}$, $l^{(i)}$, and $s^{(i)}$ are the corresponding vertical wavenumbers corresponding to the P-, T-, and S-waves, respectively. It is

$$\xi = |\kappa_1|\sin\theta_1 - \mathrm{i}|\alpha_1|\sin(\theta_1 - \gamma_1), \tag{20}$$

where θ_1 is the incidence angle and κ_1 and α_1 are given by equation 15 for incident waves with $k = k_1$ and $\gamma = \gamma_1$ (see Figure 1), and

$$d^{(i)} = D_{\mathrm{R}}^{d^{(i)}} + \mathrm{i}D_{\mathrm{I}}^{d^{(i)}}, \quad D^{d^{(i)}} = \mathrm{pv}\sqrt{(k_1^{(i)})^2 - \xi^2}, \tag{21}$$

where pv denotes the principal value, and the subscripts R and I of the complex quantity $D^{d^{(i)}}$ denote the real and imaginary parts, respectively. The calculations of $l^{(i)}$ ($D^{l^{(i)}}$) and $s^{(i)}$ ($D^{s^{(i)}}$) are similar to that of $d^{(i)}$ ($D^{d^{(i)}}$).

Subject to the boundary conditions, the displacement, stress, and temperature at the bottom of layer i can be expressed as $\mathbf{\Gamma}^{(i)} = [\,u_x^{(i)} \quad u_z^{(i)} \quad \sigma_{zz}^{(i)} \quad \sigma_{xz}^{(i)} \quad T^{(i)} \quad \bar{\kappa}T_{,z}^{(i)}\,]^{\mathrm{T}}$ ($z = h$, omitting "i" for convenience). Explicitly,

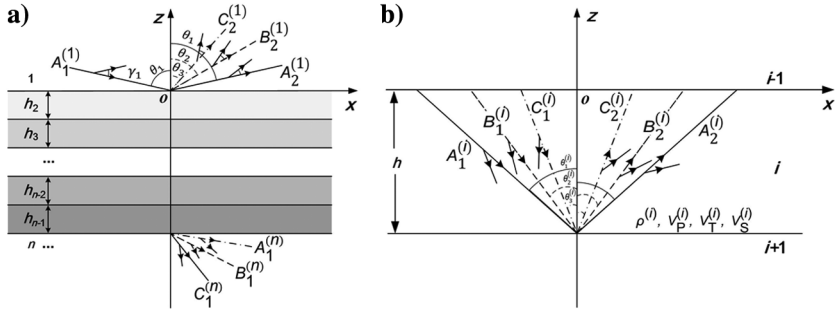

Figure 1. (a) R/T of waves in a multilayered medium and (b) details of the ith layer. The solid, dotted solid, and dashed lines represent the propagation direction of the incident P-, T-, and S-waves, respectively.

$$\mathbf{\Gamma}^{(i)} = (B_{ab}) \begin{bmatrix} A_1^{(i)} P_{\mathrm{I}}^{-1} + A_2^{(i)} P_{\mathrm{I}} \\ A_1^{(i)} P_{\mathrm{I}}^{-1} - A_2^{(i)} P_{\mathrm{I}} \\ B_1^{(i)} Q_{\mathrm{I}}^{-1} + B_2^{(i)} Q_{\mathrm{I}} \\ B_1^{(i)} Q_{\mathrm{I}}^{-1} - B_2^{(i)} Q_{\mathrm{I}} \\ C_1^{(i)} R_{\mathrm{I}}^{-1} + C_2^{(i)} R_{\mathrm{I}} \\ C_1^{(i)} R_{\mathrm{I}}^{-1} - C_2^{(i)} R_{\mathrm{I}} \end{bmatrix} e^{\mathrm{i}(\omega t - \xi x)}, \tag{22}$$

where B_{ab} are

$$\begin{cases} B_{11} = -\mathrm{i}\xi \cos P_{\mathrm{R}}, \quad B_{12} = \xi \sin P_{\mathrm{R}}, \quad B_{13} = s \sin Q_{\mathrm{R}}, \\ B_{14} = -\mathrm{i}s \cos Q_{\mathrm{R}}, \quad B_{15} = -\mathrm{i}\xi \cos R_{\mathrm{R}}, \quad B_{16} = \xi \sin R_{\mathrm{R}}; \\ B_{21} = -d \sin P_{\mathrm{R}}, \quad B_{22} = \mathrm{i}d \cos P_{\mathrm{R}}, \quad B_{23} = -\mathrm{i}\xi \cos Q_{\mathrm{R}}, \\ B_{24} = \xi \sin Q_{\mathrm{R}}, \quad B_{25} = -l \sin R_{\mathrm{R}}, \quad B_{26} = \mathrm{i}l \cos R_{\mathrm{R}}; \\ B_{31} = g_1 \cos P_{\mathrm{R}}, \quad B_{32} = \mathrm{i}g_1 \sin P_{\mathrm{R}}, \quad B_{33} = B_{34} = 0, \\ B_{35} = g_2 \cos R_{\mathrm{R}}, \quad B_{36} = \mathrm{i}g_2 \sin R_{\mathrm{R}}; \\ B_{41} = -\bar{\kappa} d g_1 \sin P_{\mathrm{R}}, B_{42} = \mathrm{i}\bar{\kappa} d g_1 \cos P_{\mathrm{R}}, \quad B_{43} = B_{44} = 0, \\ B_{45} = -\bar{\kappa} l g_2 \sin R_{\mathrm{R}}, \quad B_{46} = \mathrm{i}\bar{\kappa} l g_2 \cos R_{\mathrm{R}}; \\ B_{51} = (2\mu\xi^2 - \rho\omega^2) \cos P_{\mathrm{R}}, \quad B_{52} = (2\mu\xi^2 - \rho\omega^2)\mathrm{i} \sin P_{\mathrm{R}}, \quad B_{53} = 2\mu s \xi \mathrm{i} \sin Q_{\mathrm{R}}, \\ B_{54} = 2\mu s \xi \cos Q_{\mathrm{R}}, \quad B_{55} = (2\mu\xi^2 - \rho\omega^2) \cos R_{\mathrm{R}}, \quad B_{56} = (2\mu\xi^2 - \rho\omega^2)\mathrm{i} \sin R_{\mathrm{R}}; \\ B_{61} = 2\mu d \xi \mathrm{i} \sin P_{\mathrm{R}}, \quad B_{62} = 2\mu d \xi \cos P_{\mathrm{R}}, \quad B_{63} = \mu(s^2 - \xi^2) \cos Q_{\mathrm{R}}, \\ B_{64} = \mu(s^2 - \xi^2)\mathrm{i} \sin Q_{\mathrm{R}}, \quad B_{65} = 2\mu l \xi \mathrm{i} \sin R_{\mathrm{R}}, \quad B_{66} = 2\mu l \xi \cos R_{\mathrm{R}}, \end{cases} \tag{23}$$

and

$$\begin{aligned} &P_{\mathrm{R}} = D_{\mathrm{R}}^d h, \quad Q_{\mathrm{R}} = D_{\mathrm{R}}^s h, \quad R_{\mathrm{R}} = D_{\mathrm{R}}^l h, \\ &P_{\mathrm{I}} = \exp(D_{\mathrm{I}}^d h), \quad Q_{\mathrm{I}} = \exp(D_{\mathrm{I}}^s h), \quad R_{\mathrm{I}} = \exp(D_{\mathrm{I}}^l h), \\ &g_1 = -\frac{1}{\bar{\gamma}} ((d^2 + \xi^2)(\lambda + 2\mu) - \rho\omega^2), \\ &g_2 = -\frac{1}{\bar{\gamma}} ((l^2 + \xi^2)(\lambda + 2\mu) - \rho\omega^2), \end{aligned} \tag{24}$$

(the position of each layer refers to its bottom).

In particular, for $z = 0$, (top interface) $\mathbf{\Gamma}^{(i-1)}$ of the ith layer, matrix $\mathbf{B}$ is denoted as $(B_{ab})_{z=0}$. Let $(b_{ab})_{z=0} = [(B_{ab})_{z=0}]^{-1}$. We obtain

$$\mathbf{\Gamma}^{(i)} = (a_{ab}) \mathbf{\Gamma}^{(i-1)}, \tag{25}$$

where $a_{ab} = (B_{ab})(b_{ab})$ is the matrix of the ith layer; therefore, a_{ab} can be written as $a_{ab}^{(i)}$. We recursively get the expression of the top interface of the nth layer as

$$(\mathbf{\Gamma}^{(n)})_{z=H} = (M_{ab})(\mathbf{\Gamma}^{(1)})_{z=0}, \tag{26}$$

where

$$(M_{ab}) = \prod_{i=2}^{n-1} (a_{ab}^{(i)}), \quad H = \sum_{i=2}^{n-1} h_i, \tag{27}$$

and we assume an incident P-wave, that is,

$$B_1^{(1)} = C_1^{(1)} = A_2^{(n)} = B_2^{(n)} = C_2^{(n)} = 0. \tag{28}$$

We obtain

$$\mathbf{G} \left(\frac{P_{\mathrm{I}}^{(1)}}{A_1^{(1)}} \mathbf{\Lambda}^{\mathrm{T}} \right) = \mathbf{K}, \tag{29}$$

where

$$\begin{aligned} &\mathbf{\Lambda} = \left[A_2^{(1)} P_{\mathrm{I}}^{(1)}, \, B_2^{(1)} Q_{\mathrm{I}}^{(1)}, \, C_2^{(1)} R_{\mathrm{I}}^{(1)}, \, \frac{A_1^{(n)}}{P_{\mathrm{I}}^{(n)}}, \, \frac{B_1^{(n)}}{Q_{\mathrm{I}}^{(n)}}, \, \frac{C_1^{(n)}}{R_{\mathrm{I}}^{(n)}} \right], \\ &\mathbf{G} = (G_{ad}) = \begin{cases} d_{a(2b)} - d_{a(2b-1)}, & 1 \le d \le 3, \quad b = 1, 2, 3, \\ c_{a(2b)} + c_{a(2b-1)} & 4 \le d \le 6, \quad b = 1, 2, 3, \end{cases} \\ &\mathbf{K} = (k_{ab}) = d_{a1} + d_{a2}, \\ &\mathbf{D} = (d_{ab}) = (M_{ab})(B_{ab}^{(1)})_{z=0}, \\ &\mathbf{C} = (c_{ab}) = (B_{ab}^{(n)})_{z=H}, \end{aligned} \tag{30}$$

where $a, b, d = 1, 2, \ldots, 6$.

Similarly, for the incident S-wave,

$$A_1^{(1)} = C_1^{(1)} = A_2^{(n)} = B_2^{(n)} = C_2^{(n)} = 0, \tag{31}$$

and we obtain

$$\mathbf{G} \left(\frac{Q_{\mathrm{I}}^{(1)}}{B_1^{(1)}} \mathbf{\Lambda}^{\mathrm{T}} \right) = \mathbf{L}, \tag{32}$$

where

$$\mathbf{L} = (l_{ab}) = d_{a3} + d_{a4}. \tag{33}$$

Denoting the amplitude ratios by X_m, we express the R/T coefficients as

$$\begin{aligned} R_m &= X_m^{(1)} \frac{k_m^{(1)}}{k_0^{(1)}} = |R_m| \exp\left(\mathrm{i}\vartheta_m^{(1)}\right), \\ T_m &= X_m^{(n)} \frac{k_m^{(n)}}{k_0^{(1)}} = |T_m| \exp\left(\mathrm{i}\vartheta_m^{(n)}\right), \end{aligned} \tag{34}$$

respectively, where $k_0^{(1)}$ is the wavenumber of the incident wave; the superscripts 1 and n correspond to the incidence and transmission media, respectively, $|R_m|$ and $|T_m|$ are the amplitudes, $\vartheta_m^{(1)}$ and $\vartheta_m^{(n)}$ are the phase angles, and

$$\begin{aligned} &X_m^{(1)} = W \begin{cases} A_2^{(1)}, & m = 1, \\ B_2^{(1)}, & m = 2, \\ C_2^{(1)}, & m = 3, \end{cases} \quad X_m^{(n)} = W \begin{cases} A_1^{(n)}, \\ B_1^{(n)}, \\ C_1^{(n)}, \end{cases} \\ &W = \begin{cases} 1/A_1^{(1)}, & (\text{incident P-wave}), \\ 1/B_1^{(1)}, & (\text{incident S-wave}). \end{cases} \end{aligned} \tag{35}$$

Next, we obtain the energy fluxes to verify the R/T coefficients. Across an interface, the energy partitions are computed by using

the surface traction and particle displacement as in Carcione (2014, equation 6.115). We first consider the fluxes in media 1 (see Figure 1a):

$$\langle \mathbf{E}^{(1)} \rangle = \langle E^{(1)}_{ab} \rangle = \tfrac{1}{2}\mathrm{Re}(\mathbf{P}^{(1)}_{4\times 2} \cdot \dot{\tilde{\mathbf{Q}}}^{(1)}_{2\times 4}), \quad (a,b=0,1,2,3), \tag{36}$$

where the diagonal element $\langle E^{(1)}_{00} \rangle$ is the energy flux of the incident wave; $\langle E_{11} \rangle$, $\langle E_{22} \rangle$, and $\langle E_{33} \rangle$ correspond to the reflected P-, T-, and S-waves, respectively, with $\langle \cdot \rangle$ denoting a temporal average over a period; and the bar over a quantity denotes the complex conjugate. The presence of the off-diagonal parts indicates the interference energy fluxes between the incident and reflected waves, and

$$P^{(1)}_{m1} = \left(\sigma^{(1)}_{zz}\right)_m, \quad P^{(1)}_{m2} = \left(\sigma^{(1)}_{xz}\right)_m, \quad Q^{(1)}_{1m} = \left(u^{(1)}_z\right)_m,$$
$$Q^{(1)}_{2m} = \left(u^{(1)}_x\right)_m, \quad (m=0,1,2,3), \tag{37}$$

where the subscripts $m = 0$, 1, 2, and 3 correspond to the incident, reflected P-, T-, and S-waves, respectively.

Similarly, the energy fluxes of the transmitted waves are

$$\langle \mathbf{E}^{(n)} \rangle = \left\langle E^{(n)}_{ab} \right\rangle = \tfrac{1}{2}\mathrm{Re}\left(\mathbf{P}^{(n)}_{3\times 2} \cdot \dot{\tilde{\mathbf{Q}}}^{(n)}_{2\times 3}\right), \quad (a,b=4,\ldots,6), \tag{38}$$

where $\langle E^{(n)}_{44} \rangle$, $\langle E^{(n)}_{55} \rangle$, and $\langle E^{(n)}_{66} \rangle$ correspond to the P-, T-, and S-waves, respectively; the off-diagonal entries are the interference energy fluxes between the waves; and $P^{(n)}_{m1}$, $P^{(n)}_{m2}$, $Q^{(n)}_{m1}$, and $Q^{(n)}_{m2}$ ($m = 1$, 2, and 3) are similar to equation 37 but for the transmitted waves.

Then, the energy ratios are

$$E^{\mathrm{i}}_{ab} = \frac{\left\langle E^{(1)}_{ab} \right\rangle}{\langle E_{00} \rangle}, \quad (a,b=0,1,2,3),$$
$$E^{\mathrm{t}}_{ab} = \frac{\left\langle E^{(n)}_{ab} \right\rangle}{\langle E_{00} \rangle}, \quad (a,b=4,5,6), \tag{39}$$

and the energy balance is (Carcione, 2014, equation 6.116; Wang et al., 2020a)

$$E_{\mathrm{sum}} = \sum_{a=1}^{3}\left(E^{\mathrm{i}}_{a0} + E^{\mathrm{i}}_{0a} + \sum_{b=1}^{3} E^{\mathrm{i}}_{ab}\right) + \sum_{a=4}^{6}\sum_{b=4}^{6} E^{t}_{ab} = -1,$$
$$E_{\mathrm{in}} = E_{\mathrm{ir}} + E_{\mathrm{t}} = \sum_{a=0}^{3}\left(\sum_{b=0}^{3} E^{\mathrm{i}}_{ab} - E^{\mathrm{i}}_{aa}\right) + \sum_{a=4}^{6}\left(\sum_{b=4}^{6} E^{t}_{ab} - E^{t}_{aa}\right), \tag{40}$$

where E_{sum} is the sum of the energy ratios, E_{in} is the interference energy ratio, E_{ir} corresponds to the interaction between the incident and the reflected waves, and E_{t} corresponds to the interaction among the transmitted waves.

EXAMPLES

We first analyze the dispersion relation and compare elastic and thermoelastic models to verify the R/T coefficients. The properties of the media ($n = 1$ and 2 in this case) are given in Table 1 (Schon, 2011; Guo et al., 2020).

Plane-wave analysis

Thermal effects cause attenuation and imply complex wavenumbers and inhomogeneous waves. The phase velocities and attenuation coefficients of the two P-waves based on the LS theory as a function of frequency for two values of the inhomogeneity angle are shown in Figure 2; the γ has a negligible influence on the dispersion at seismic frequencies because the imaginary part of k is relatively small (equation 15), where the T-wave velocity is almost zero and the attenuation is very high. The T mode is lossless

Table 1. Medium properties.

Medium, n	1	2	3	4	4′
V_0 (km/s)	3.05	3.73	4.2	4.5	4.7
V_S (km/s)	1.76	2.15	2.43	2.6	2.71
Density, ρ (kg/m^3)	2000	2150	2340	2870	2410
Specific heat, c (J/(kg·K))	900	910	920	980	930
Thermal conductivity, $\bar{\kappa}$ (W/(m·K))	2.9	2.8	2.7	3.6	2.6
Coefficient of thermal expansion, $\bar{\alpha}$ ($\times 10^{-6}$ K^{-1})	1.7	1.8	1.9	1.4	2.0
Absolute temperature, T_0 (K)	300	310	320	450	330

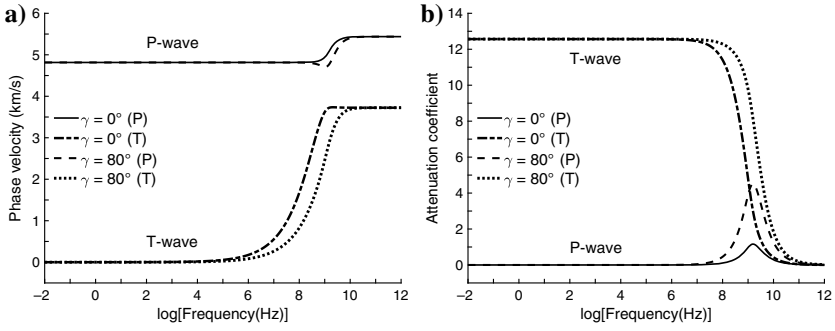

Figure 2. (a) Phase velocity and (b) attenuation coefficient as a function of frequency for two values of the inhomogeneity angle γ, where the medium properties correspond to $n = 4$ in Table 1.

DOI:10.1190/geo2021-0542.1

and wave-like only at very high frequencies. The low-frequency phase velocities of the P-waves are 3125 ($n = 1$), 3898 ($n = 2$), 4490 ($n = 3$), 4815 ($n = 4$), and 5172 m/s ($n = 4'$), respectively, according to Table 1 and equation 16. Meanwhile, the low-frequency behaviors and values of P-waves here also are applicable to the classic thermoelastic model and independent of the thermal properties according to Hou et al. (2021b). The relaxation frequency is approximately

$$f_r = 1/(2\pi\tau), \tag{41}$$

where we have assumed (Carcione et al., 2019a)

$$\tau = \bar{\kappa}/(cV_0), \tag{42}$$

where τ represents the time lag to establish a steady-state heat conduction in an element of volume. It depends on the thermal properties and has little effect at low frequencies (Hou et al., 2021b). Moreover, the fast P-wave relaxation peaks due to the thermal effects are located at high frequencies (gigahertz range), whereas the S-wave is not affected.

R/T coefficients

Figure 3 depicts the absolute values of the R/T coefficients as a function of the incidence angle for a frequency of 10 Hz, in the case of an incident P-wave, where R_{PP} and R_{PS} denote the reflection coefficients of the P- and S-waves, and T_{PP} and T_{PS} those of the transmitted waves. At 10 Hz, the influence of the inhomogeneity angle on the phase velocity and attenuation are negligible (see Figure 2), and consequently, we set $\gamma = 0°$ (homogeneous wave). Because the velocity of the S-wave is much lower than that of the P-wave (see Figure 2 and Table 1), the amplitudes of the reflected and transmitted S-waves are relatively small.

For many layers, we implement the TM method based on the LS theory, where n is defined in Figure 1a. For n equals three or four, besides the two half-spaces (upper and lower media), we have one and two layers, respectively, each assumed with 80 m thickness. The properties of the media are specified in Table 1, where the lower half-space (medium 4) is an HDR geothermal resource with high thermal conductivity and absolute temperature. The corresponding phase angles are displayed in Figure 4. We compute the energy balance according to amplitude ratios (R/T coefficients) (equation 35) and obtain $E_{sum} = -1$ (equation 40) to verify coefficient results (Wang et al., 2020a, 2021). Moreover, it can be confirmed that the sum of the P- and S-wave ratios calculated by equation 39 satisfies the verification conditions because the phase velocity of the T-wave at seismic frequencies is almost zero and the attenuation is high, implying negligible energy. An S-wave is not generated at normal incidence. In the following, we show the R/T of the corresponding elastic (isothermal and lossless) case. Differences with the previous curves are due to the thermal effects. Comparison of Figures 3 and 5 shows that the amplitude (energy) of the reflected and transmitted S-waves is higher in the elastic case. Figure 6 displays the corresponding phase angles of the thermoelastic case. A direct comparison between the thermoelastic and isothermal (elastic) cases is shown in Figure 7. Similar plots for an incident S-wave are shown in Figures 8 and 9 (thermoelastic case) and Figures 10 and 11 (elastic case).

Effect of the thermal properties

Now, we consider the effect of thermal properties by comparing the cases $n = 4$ (HDR) with $n = 4'$ in Table 1, where the model consists of two half-spaces (upper and lower media) and two layers of 80 m thickness. Figure 12 shows the R/T coefficients for an incident P-wave, where, as expected, there is no S-wave at normal incidence. Varying the temperature and thermal parameters affects the velocities of the waves calculated by equation 16. The HDR temperature hardly affects the amplitude of the reflected P-wave,

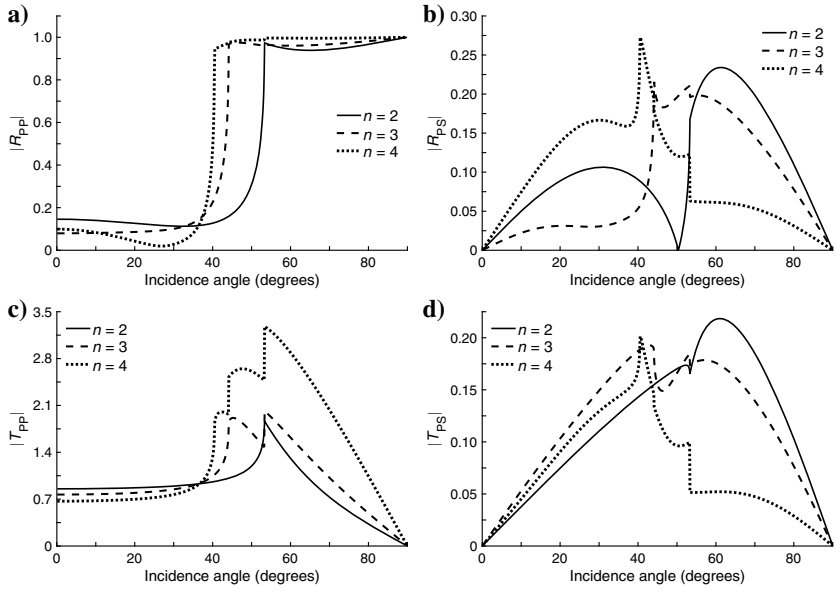

Figure 3. The coefficients of the (a) reflected P-, (b) reflected S-, (c) transmitted P- and (d) transmitted S-waves versus incidence angle θ for an incident P-wave at 10 Hz. The n is defined in Figure 1a, and the medium properties are defined in Table 1.

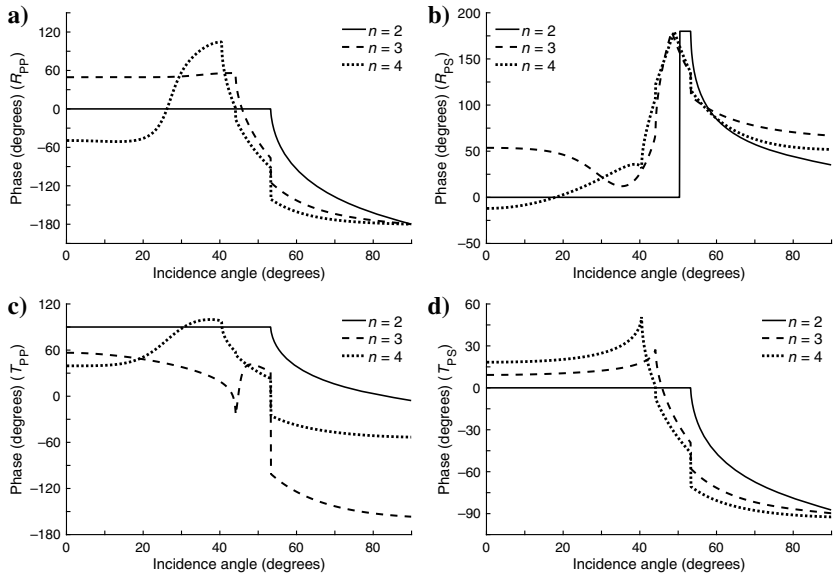

Figure 4. Phase angles corresponding to Figure 3.

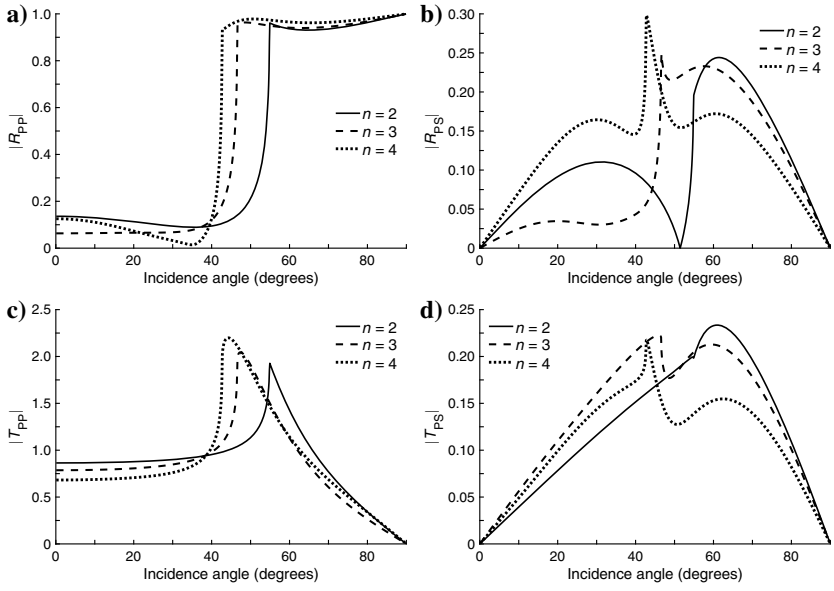

Figure 5. The coefficients of the (a) reflected P-, (b) reflected S-, (c) transmitted P- and (d) transmitted S-waves for the elastic models and an incident P-wave.

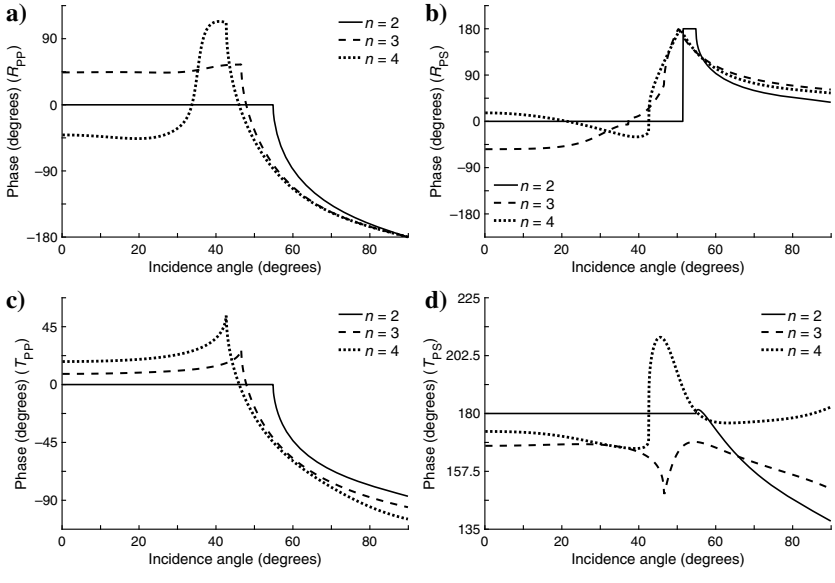

Figure 6. Phase angles corresponding to Figure 5.

Figure 7. Comparison of reflection coefficients and phase angles for (a and c) reflected P and (b and d) reflected S between thermoelastic (the solid lines) and elastic (the dashed lines) cases as a function of the P-wave incidence angle, where $f = 10$ Hz and $n = 4$.

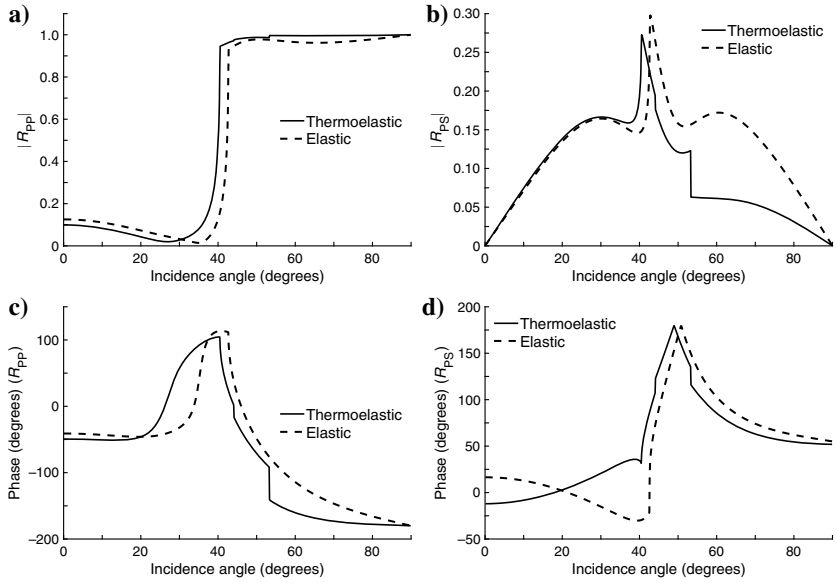

Figure 8. The coefficients of the (a) reflected P-, (b) reflected S-, (c) transmitted P- and (d) transmitted S-waves versus incidence angle θ for an incident S-wave at 10 Hz. The n is defined in Figure 1a and the medium properties are defined in Table 1.

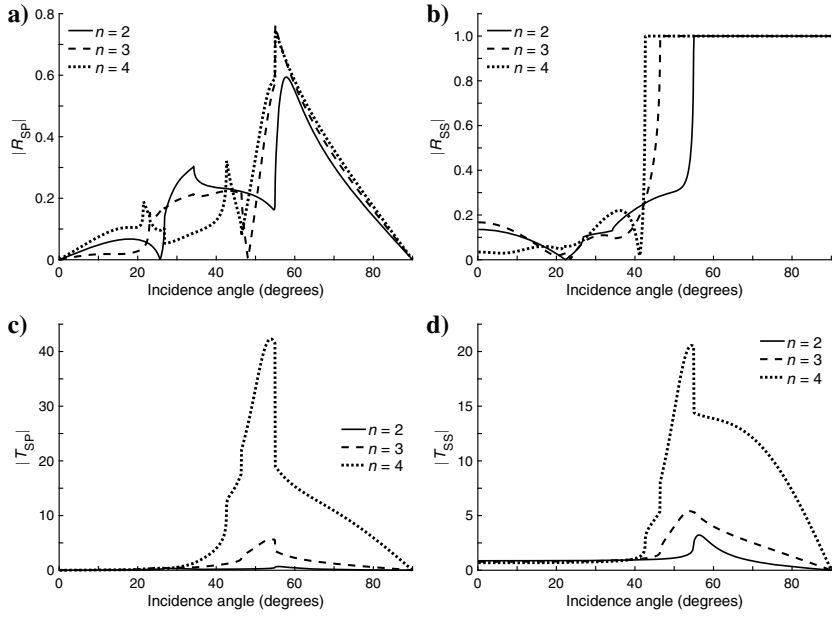

Figure 9. Phase angles corresponding to Figure 8.

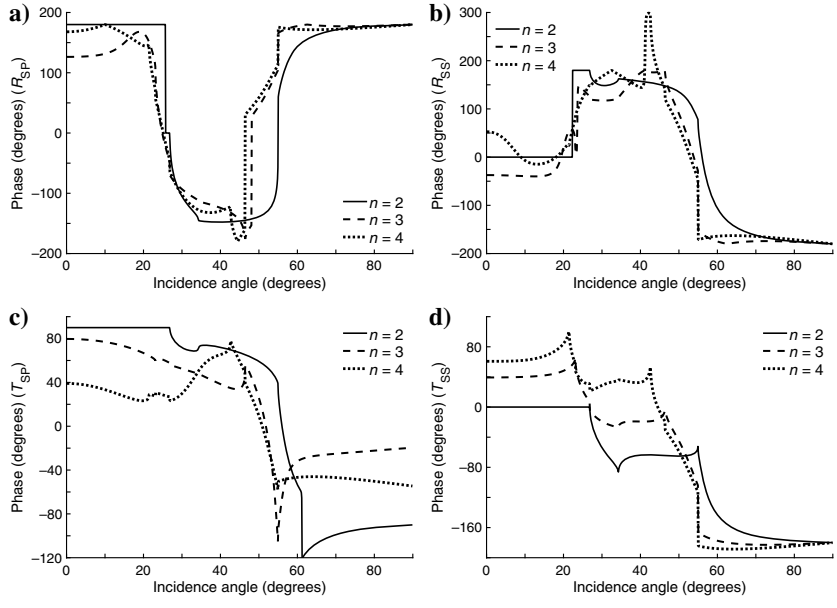

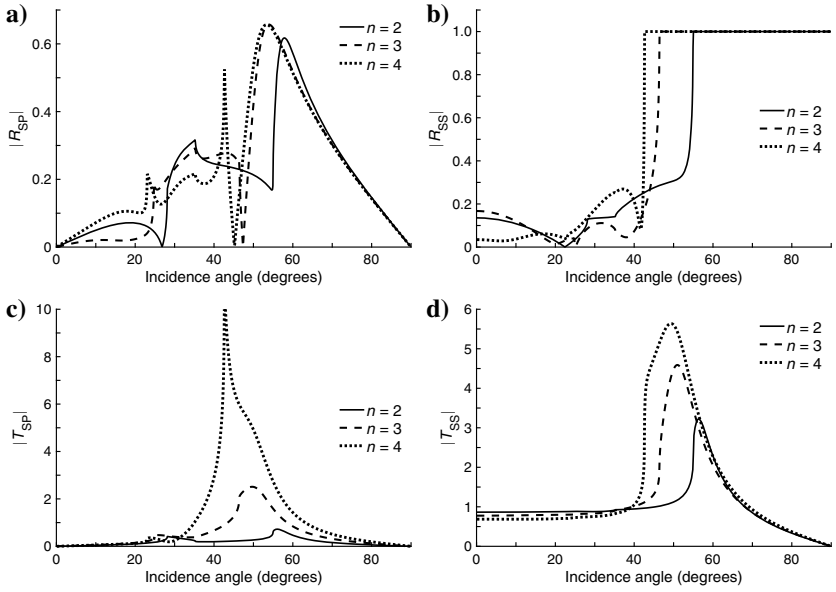

Figure 10. The coefficients of the (a) reflected P-, (b) reflected S-, (c) transmitted P- and (d) transmitted S-waves for the elastic models and an incident S-wave.

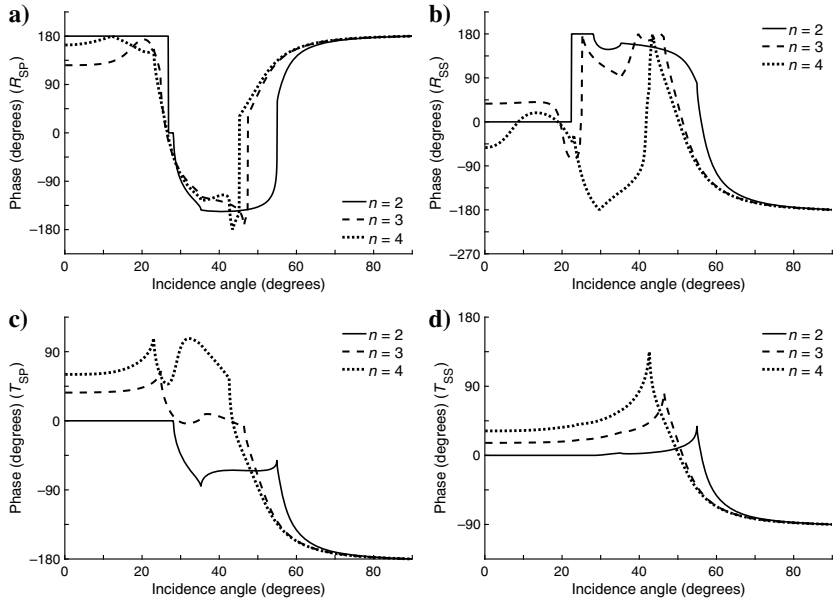

Figure 11. Phase angles corresponding to Figure 10.

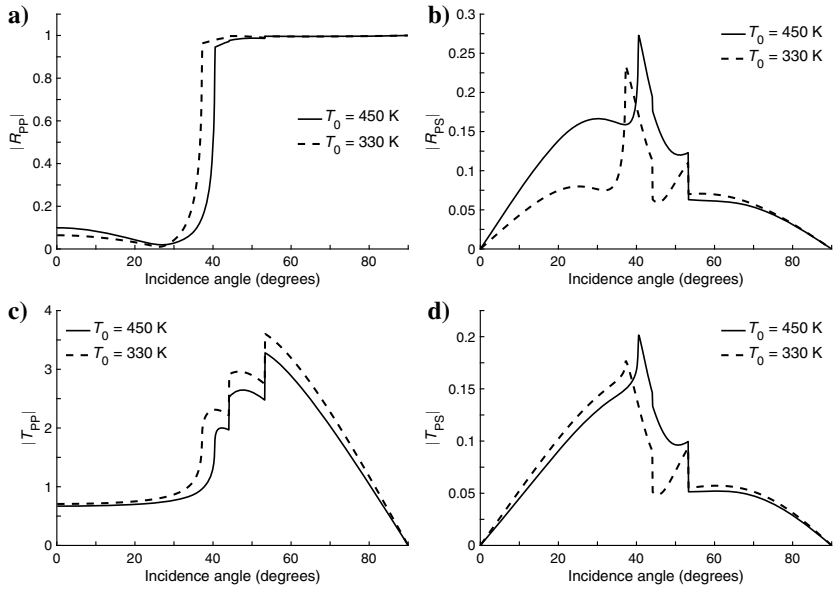

Figure 12. The coefficients of the (a) reflected P-, (b) reflected S-, (c) transmitted P- and (d) transmitted S-waves versus incidence angle θ for an incident P-wave at 10 Hz, where the medium properties of $T_0 = 330$ K correspond to the last column in Table 1 ($n = 4'$). The n is defined in Figure 1a, and the medium properties are defined in Table 1.

Figure 13. Phase angles corresponding to Figure 12.

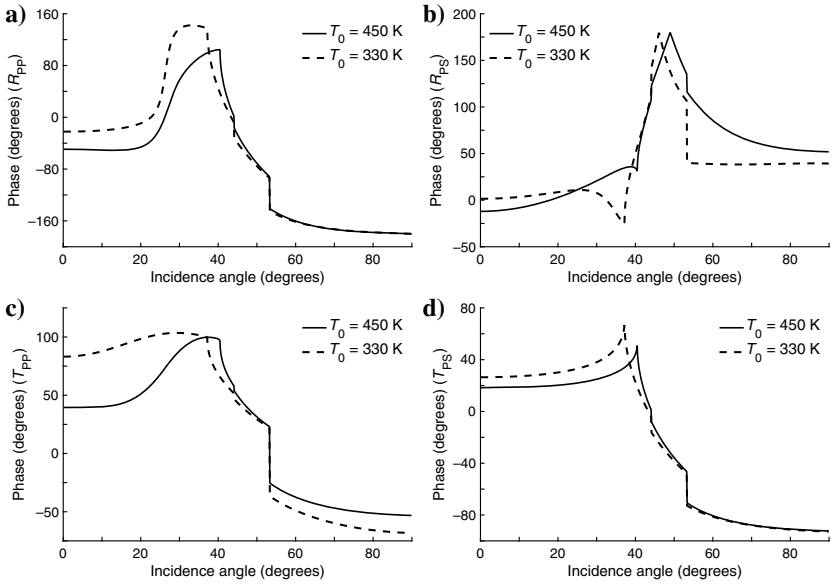

Figure 14. The coefficients of the (a) reflected P-, (b) reflected S-, (c) transmitted P- and (d) transmitted S-waves versus incidence angle θ for an incident P-wave, where the frequency is variable and $n = 4$ is defined in Table 1.

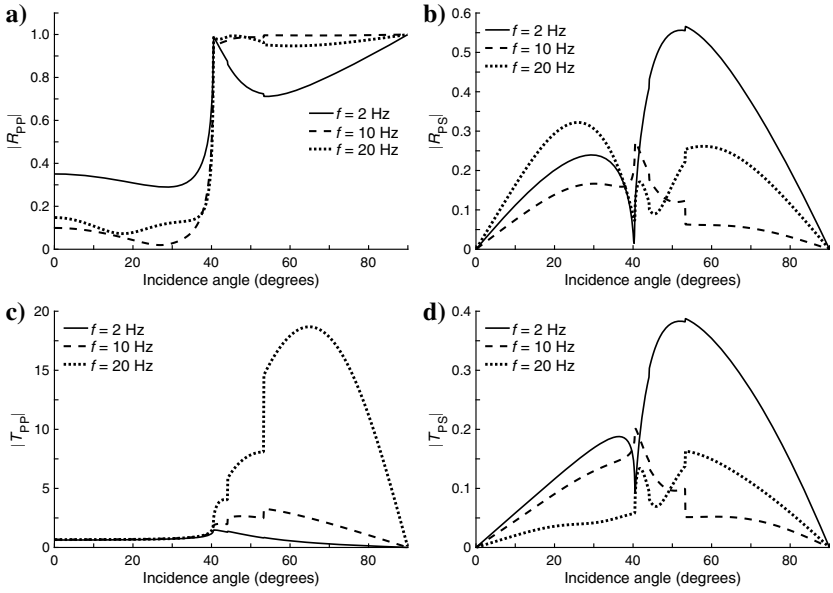

Figure 15. Phase angles corresponding to Figure 14.

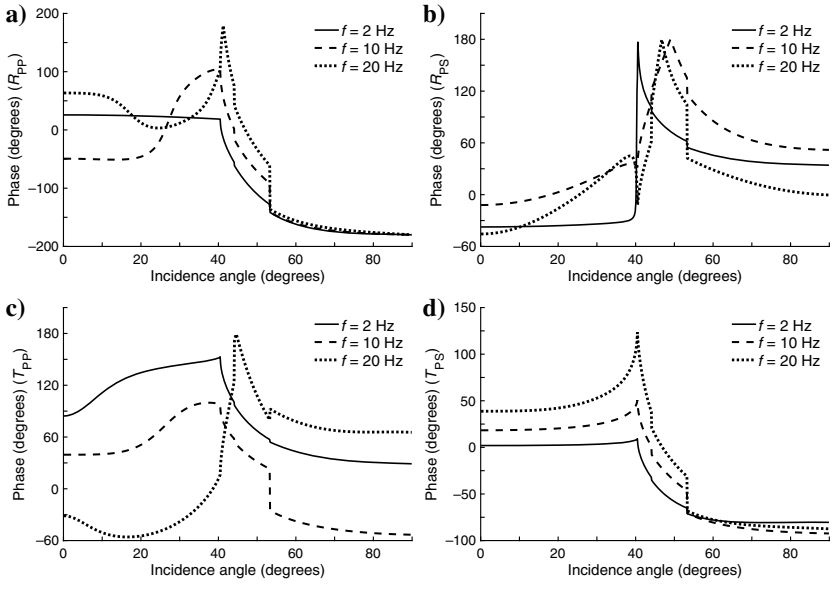

and the most relevant effects are the increase in R_{PS} and T_{PS} with increasing T_0. Figure 13 shows the corresponding phases.

Effect of the frequency and layer thickness

Figure 2 indicates that the phase velocities and attenuation of $n = 4$ and $4'$ are practically similar at low frequencies. As an example, Figures 14 and 15 show the R/T amplitudes and phase angles as a function of the incidence angle for an incident P-wave, respectively, where we observe that the critical angle is independent of frequency and that with decreasing frequency, the amplitudes of the converted S-wave are enhanced. As the layer thickness increases, the curves (Figures 16 and 17) show more pronounced inflection points and peaks. The R/T coefficients behave as a frequency filtering effect in thermoelastic multilayered media.

CONCLUSION

We have applied a novel TM algorithm to obtain the R/T coefficients of thermoelastic waves in multilayered media, in which the stress-strain relations are based on the LS theory. Because the presence of dissipation due to thermal effects makes the wave inhomogeneous, the direction of propagation and attenuation of the different modes does not necessarily coincide. However, the influence of inhomogeneity is negligible at seismic frequencies where, analogously to the Biot slow P-wave in poroelasticity, the T-wave is diffusive. The thermoelastic coefficients are compared to those of the elastic (lossless) case, which shows how the amplitudes and phase angles are affected by the thermal properties. The coefficients are verified by an energy balance. The example considers an HDR geothermal field with different absolute temperatures, frequencies,

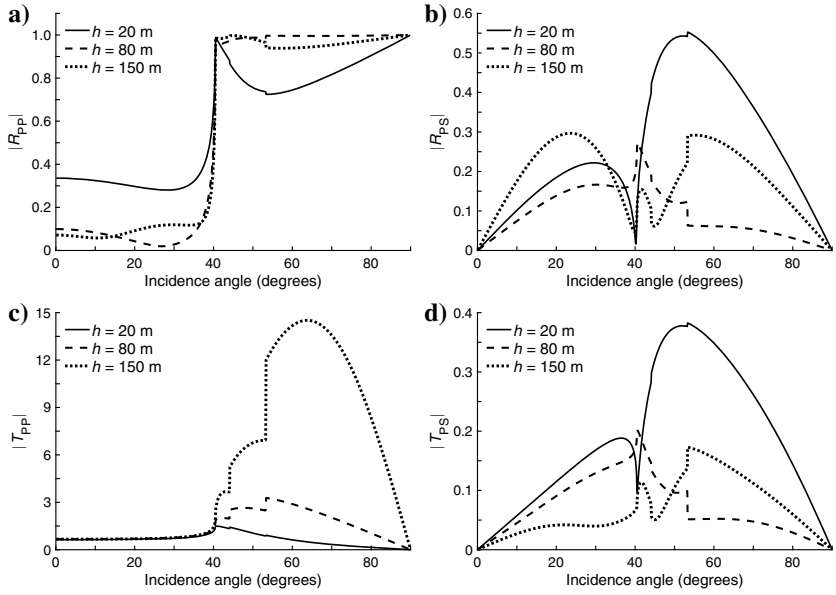

Figure 16. The coefficients of the (a) reflected P-, (b) reflected S-, (c) transmitted P- and (d) transmitted S-waves versus incidence angle θ for an incident P-wave and different layer thicknesses of media 2 and 3.

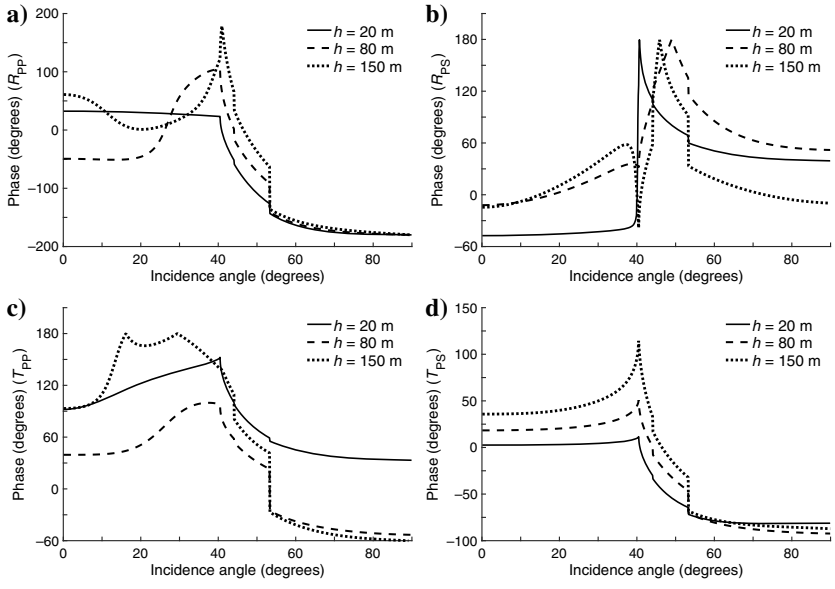

Figure 17. Phase angles corresponding to Figure 16.

and layer thicknesses of the cap rocks. The coefficients of the reflected and transmitted P-waves for different temperatures are similar, whereas the amplitudes of the S-waves are higher for higher temperatures. The reflection coefficients can be used to obtain information about the thermal characteristics of a multilayered medium, which provides theoretical support for HDR geothermal exploration.

ACKNOWLEDGMENTS

The research is supported by the National Natural Science Foundation of China (grant no. 41821002) and 111 project "Deep-Superdeep Oil & Gas Geophysical Exploration" (B18055).

DATA AND MATERIALS AVAILABILITY

Data associated with this research are available and can be obtained by contacting the corresponding author.

REFERENCES

Ackerman, C. C., B. Bertman, H. A. Fairbank, and R. A. Guyer, 1966, Second sound in solid helium: Physical Review Letters, **16**, 789–791, doi: 10.1103/PhysRevLett.16.789.

Ai, Z. Y., L. J. Wang, and K. Zeng, 2015, Analytical layer-element method for 3D thermoelastic problem of layered medium around a heat source: Meccanica, **50**, 49–59, doi: 10.1007/s11012-014-0049-0.

Bahar, L. Y., 1972, Transfer matrix approach to layered systems: Journal of the Engineering Mechanics Division, **98**, 1159–1172, doi: 10.1061/JMCEA3.0001660.

Bahar, L. Y., and R. B. Hetnarski, 1980, Coupled thermoelasticity of a layered medium: Journal of Thermal Stresses, **3**, 141–152, doi: 10.1080/01495738008926958.

Biot, M. A., 1956, Thermoelasticity and irreversible thermodynamics: Journal of Applied Physics, **27**, 240–253, doi: 10.1063/1.1722351.

Boschi, E., 1973, A thermoviscoelastic model of the earthquake source mechanism: Journal of Geophysical Research, **78**, 7733–7737, doi: 10.1029/JB078i032p07733.

Brown, D. W., D. V. Duchane, G. Heiken, and V. T. Hriscu, 2012, Mining the earth's heat: Hot dry rock geothermal energy: Springer-Verlag.

Bufler, H., 1971, Theory of elasticity of a multilayered medium: Journal of Elasticity, **1**, 125–143, doi: 10.1007/BF00046464.

Carcione, J. M., 2014, Wave fields in real media. Theory and numerical simulation of wave propagation in anisotropic, anelastic and porous media, 3rd ed.: Elsevier.

Carcione, J. M., F. Cavallini, E. Wang, J. Ba, and L. Y. Fu, 2019b, Physics and simulation of wave propagation in linear thermo-poroelastic media: Journal of Geophysical Research, **124**, 8147–8166, doi: 10.1029/2019JB017851.

Carcione, J. M., Z. W. Wang, W. Ling, E. Salusti, J. Ba, and L. Y. Fu, 2019a, Simulation of wave propagation in linear thermoelastic media: Geophysics, **84**, no. 1, T1–T11, doi: 10.1190/geo2018-0448.1.

Chakraborty, N., and M. C. Singh, 2011, Reflection and refraction of a plane thermoelastic wave at a solid–solid interface under perfect boundary condition, in presence of normal initial stress: Applied Mathematical Modelling, **35**, 5286–5301, doi: 10.1016/j.apm.2011.04.026.

Deresiewicz, H., 1957, Plane waves in a thermoelastic solid: Journal of the Acoustical Society of America, **29**, 204–209, doi: 10.1121/1.1908832.

Eslami, M. R., R. B. Hetnarski, J. Ignaczak, N. Noda, N. Sumi, and Y. Tanigawa, 2013, Theory of elasticity and thermal stresses: Springer Netherlands.

Green, A. E., and K. A. Lindsay, 1972, Thermoelasticity: Journal of Elasticity, **2**, 1–7, doi: 10.1007/BF00045689.

Guo, T., S. Tang, S. Liu, X. Liu, and G. Qu, 2020, Numerical simulation of hydraulic fracturing of hot dry rock under thermal stress: Engineering Fracture Mechanics, **240**, 107350–107370, doi: 10.1016/j.engfracmech.2020.107350.

Haskell, N. A., 1953, The dispersion of surface waves on multilayered media: Bulletin of the Seismological Society of America, **43**, 17–34, doi: 10.1785/BSSA0430010017.

Hou, W., L. Y. Fu, J. M. Carcione, Z. W. Wang, and J. Wei, 2021a, Simulation of thermoelastic waves based on the Lord-Shulman theory: Geophysics, **86**, no. 3, T155–T164, doi: 10.1190/geo2020-0515.1.

Hou, W., L. Y. Fu, J. Wei, and Z. W. Wang, 2021b, Characteristics of wave propagation in thermoelastic medium: Chinese Journal of Geophysics (in Chinese), **64**, 1364–1374.

Ignaczak, J., and M. Ostoja-Starzewski, 2009, Thermoelasticity with finite wave speeds: OUP Oxford.

Jacquey, A. B., M. Cacace, G. Blöcher, and M. Scheck-Wenderoth, 2015, Numerical investigation of thermoelastic effects on fault slip tendency during injection and production of geothermal fluids: Energy Procedia, **76**, 311–320, doi: 10.1016/j.egypro.2015.07.868.

Kaur, I., P. Lata, and K. Singh, 2020, Reflection and refraction of plane wave in piezo-thermoelastic diffusive half spaces with three phase lag memory dependent derivative and two-temperature: Waves in Random and
Complex Media, **2**, 1–34, doi: 10.1080/17455030.2020.1856451.

Lord, H. W., and Y. Shulman, 1967, A generalized dynamical theory of thermoelasticity: Journal of the Mechanics and Physics of Solids, **15**, 299–309, doi: 10.1016/0022-5096(67)90024-5.

McNelly, T. F., S. J. Rogers, D. J. Channin, R. J. Rollefson, W. M. Goubau, G. E. Schmidt, J. A. Krumhansl, and R. O. Pohl, 1970, Heat pulses in NaF: onset of second sound: Physical Review Letters, **24**, 100–102, doi: 10.1103/PhysRevLett.24.100.

Nowacki, W., 1975, Dynamic problems of thermoelasticity: Springer Netherlands.

Potel, C., and J. F. D. Belleval, 1993, Propagation in an anisotropic periodically multilayered medium: The Journal of the Acoustical Society of America, **93**, 2669–2677, doi: 10.1121/1.405842.

Rudgers, A. J., 1990, Analysis of thermoacoustic wave propagation in elastic media: The Journal of the Acoustical Society of America, **88**, 1078–1094, doi: 10.1121/1.399856.

Schon, J. H., 2011, Physical properties of rocks: A workbook: Elsevier.

Sinha, S. B., and K. A. Elsibai, 1996, Reflection of thermoelastic waves at a solid half-space with two relaxation times: Journal of Thermal Stresses, **19**, 749–762, doi: 10.1080/01495739608946205.

Tehrani, P. H., and R. Mohamad, 2000, Boundary element analysis of Green and Lindsay theory under thermal and mechanical shock in a finite domain: Journal of Thermal Stresses, **23**, 773–792, doi: 10.1080/01495730050192400.

Thomson, W. T., 1950, Transmission of elastic waves through a stratified solid medium: Journal of Applied Physics, **21**, 89–93, doi: 10.1063/1.1699629.

Vashishth, A. K., and P. Khurana, 2004, Waves in stratified anisotropic poroelastic media: A transfer matrix approach: Journal of sound and vibration, **277**, 239–275, doi: 10.1016/j.jsv.2003.08.024.

Wang, E., J. M. Carcione, J. Ba, and Y. Liu, 2020a, Reflection and transmission of plane elastic waves at an interface between two double-porosity media: Effect of local fluid flow: Surveys in Geophysics, **41**, 283–322, doi: 10.1007/s10712-019-09572-6.

Wang, E., J. M. Carcione, Y. Yuan, and J. Ba, 2021, Reflection of inhomogeneous plane waves at the surface of a thermo-poroelastic medium: Geophysical Journal International, **224**, 1621–1639, doi: 10.1093/gji/ggaa543.

Wang, Z. W., L. Y. Fu, J. Wei, W. Hou, J. Ba, and J. M. Carcione, 2020b, On the Green function of the Lord-Shulman thermoelasticity equations: Geophysical Journal International, **220**, 393–403, doi: 10.1093/gji/ggz453.

Biographies and photographs of the authors are not available.